ISSN 1674-1056
http://cpb.iphy.ac.cn
http://iopscience.iop.org/cpb
中国物理 B
Chinese Physics
中国物理
Chinese Physics B

Acoustic characteristics of pulse detonation engine with ellipsoidal reflector

Yang Kang(康杨), Ning Li(李宁), Chun-Sheng Weng(翁春生), Chuan-Wei Wang(王传位)

Citation: Chin. Phys. B . 2018, 27(10): 104703. **doi:** 10.1088/1674-1056/27/10/104703

Journal homepage: http://cpb.iphy.ac.cn; http://iopscience.iop.org/cpb

What follows is a list of articles you may be interested in

Three-dimensional detonation cellular structures in rectangular ducts using an improved CESE scheme

Yang Shen(沈洋), Hua Shen(申华), Kai-Xin Liu(刘凯欣), Pu Chen(陈璞), De-Liang Zhang(张德良)
Chin. Phys. B . 2016, 25(11): 114702. **doi:** 10.1088/1674-1056/25/11/114702

Critical deflagration waves leading to detonation onset under different boundary conditions

Lin Wei, Zhou Jin, Fan Xiao-Hua, Lin Zhi-Yong
Chin. Phys. B . 2015, 24(1): 014701. **doi:** 10.1088/1674-1056/24/1/014701

Particle path tracking method in two-and three-dimensional continuously rotating detonation engines

Zhou Rui, Wu Dan, Liu Yan, Wang Jian-Ping
Chin. Phys. B . 2014, 23(12): 124704. **doi:** 10.1088/1674-1056/23/12/124704

Existence of a Hartmann layer in the peristalsis of Sisko fluid

Saleem Asghar, Tayyaba Minhas, Aamir Ali
Chin. Phys. B . 2014, 23(5): 054702. **doi:** 10.1088/1674-1056/23/5/054702

Acoustic characteristics of bubble bursting at the surface of a high-viscosity liquid

Liu Xiao-Bo,Zhang Jian-Run,Li Pu
Chin. Phys. B . 2012, 21(5): 054301. **doi:** 10.1088/1674-1056/21/5/054301

Acoustic characteristics of pulse detonation engine with ellipsoidal reflector*

Yang Kang(康杨), Ning Li(李宁)†, Chun-Sheng Weng(翁春生), and Chuan-Wei Wang(王传位)

National Key Laboratory of Transient Physics, Nanjing University of Science and Technology, Nanjing 210094, *China*

(Received 7 May 2018; revised manuscript received 14 July 2018; published online 10 September 2018)

Acoustic characteristics of a pulse detonation engine (PDE) with and without an ellipsoidal reflector are numerically and experimentally investigated. A two-dimensional (2D) non-splitting unstructured triangular mesh Euler solver based on the space-time conservation element and solution element (CE/SE) method is employed to simulate the flow field of a PDE. The numerical results clearly demonstrate the external flow field of the PDE. The effect of an ellipsoidal reflector on the flow field characteristic near the PDE exit is investigated. The formation process of reflected shock wave and reflected jet shock are reported in detail. An acoustic measurement system is established for the PDE acoustic testing. The experimental results show that the ellipsoidal reflector changes the sound waveform and directivity of PDE sound. The reflected shock wave and reflected jet shock result in two more positive pressure peaks in the sound waveform. The ellipsoidal reflector changes the directivity of PDE sound from 20° to 0°. It is found that the peak sound pressure level (PSPL) and overall sound pressure level (OASPL) each obtain an increment when the PDE is installed with a reflector. The maximum relative increase ratio of PSPL and OASPL are obtained at the focus point F_2, whose values are 6.1% and 6.84% respectively. The results of the duration of the PDE sound indicate that the reflecting and focusing wave generated by the reflector result in the increment of A duration and B duration before and near focus point F_2. Results show that the ellipsoidal reflector has a great influence on the acoustic characteristic of PDE sound. The research is helpful for understanding the influence of an ellipsoidal reflector on the formation and propagation process of PDE sound.

Keywords: pulse detonation engine, ellipsoidal reflector, acoustic characteristics, experiments and simulations

PACS: 47.40.Rs, 43.25.Jh, 43.28.Mw **DOI:** 10.1088/1674-1056/27/10/104703

1. Introduction

The pulse detonation engine (PDE) is an innovative propulsion technology that could potentially provide significant advantages, such as mechanical simplicity, higher thrust-to-weight ratio, lower cost, high thermodynamic cycle efficiency, and a wide working scope. Much progress has been made in many important performance aspects of PDEs.[1] In order for the PDE to be commercially successful as a propulsion device, the environmental effect of the PDE should be considered as an important issue. When the detonation products are directly exhausted from the detonation chamber to the ambient environment, part of the chemistry energy of fuel is converted into acoustic energy instead of being converted into the kinetic energy to produce thrust. However, relatively few researches have been published on PDE acoustics. The preliminary studies provided an initial understanding of PDE acoustic behavior.[2–9] The PDE sound is produced by two sources: noise associated with the shock wave, and jet noise produced during the blowdown of hot detonation products.[10] The definition of impulsive noise was brought forward in a China National Standard of GJB50-85, namely, the noise which is composed of one or more abrupt noises (its duration time is less than 1 s) can be called impulsive noise. According to its physical characteristics, the impulsive noise can be classified as two kinds. One is the impact noise, which is caused by solid objects impacting, the elasticity vibration, distortion, and rupture, and the other is caused by pulsed pressure which is produced by blast, bang, or turbulence. Obviously, the PDE noise belongs to impulsive noise. The sound radiation characteristics of PDE sound are intermittent, periodic short duration, and high intensity. The noise and vibrations generated by the PDE directly affect aircraft stealth and structure fatigue, thus posing a serious threat to the overall performance and safety of aircraft. It has been suggested that the ellipsoidal reflector used can gather part of the sound energy to the action target, otherwise this energy would radiate to other places. This utility of the ellipsoidal reflector can be used to reduce the noise impact of critical parts of the PDE. The ability of the ellipsoidal reflector to focus acoustic energy will make PDEs have important application prospects in other military fields.

In general, there are three ways to focus sound waves.[11,12] The first is the phased array method. By adjusting parameters such as the delay time, spacing, and emission frequency of each array element, acoustic beams with small side lobes and strong directivity can be formed, thereby forming high-energy beam spot areas at the target point. The phased

*Project supported by the National Natural Science Foundation of China (Grant Nos. 11372141 and 11472138) and the National Defense Pre-Research Foundation of China (Grant No. 61426040201162604002).

†Corresponding author. E-mail: phoenixkyo@163.com

© 2018 Chinese Physical Society and IOP Publishing Ltd

array can realize the multi-point focusing and any angle deflection of the sound beam without an auxiliary mechanical rotating device. The second is the acoustic lens method. By using special materials and design structures, the acoustic wave bends when it passes through the lens, thus achieving a higher intensity at the target point. The third is the surface reflection method. The originally spherical diffused sound wave is reflected as a convergent wave through a curved reflector with special geometric properties, such as rotating parabolic surface and ellipsoid.

Compared with the former two types of acoustic energy accumulation, the reflective energy accumulation is relatively simple. The acoustic energy can be enhanced at the target point by installing a reflector with a special geometry on the sound source. Cates and Sturtevant[13,14] developed a finite-difference numerical method for geometrical shock dynamics based on the analogy between the nonlinear ray equations and the supersonic potential equation. The numerical results exhibited the qualitative behavior of strong, moderate, and weak shock focusing observed experimentally. The results showed that the maximum pressure at focus is influenced by the aperture angle and shock strength. Schaefer and Grapperhaus[15] measured the light and sound emitted by an air sparker-reflector combination. The quantitative measurement results combined with a reflector model indicated that the reflector directs and focuses the sound to deliver high intensity pulses at range. Zhou and Zhong[16] explored the effect of reflector geometry on the acoustic field produced by an electrohydraulic shock wave lithotripter. The pressure wave form generated by the spark discharge was measured and used as a source condition in numerical calculations. An equivalent reflector model was developed and proved to be a useful tool for the prediction of pressure wave form generated in a lithotripter field. However, there is no report on the application of reflectors to PDE sound.

In this study, experimental and computational investigations are performed on a PDE with and without an ellipsoidal reflector. The effects of the ellipsoidal reflector on PDE acoustic characteristics are explored. The acoustic characteristics of PDE, including peak sound pressure level (PSPL), overall sound pressure level (OASPL), directivity and duration, are analyzed. The simulated results can enhance the understanding of acoustic formation mechanisms of PDE sound. It is found that the reflector can reflect and focus the most acoustic energy, which originally points to the upstream direction, in the vicinity of the reflector focus. The installation of the reflector does not enlarge the area affected by PDE sound.

2. Experimental measurement and computational analysis

2.1. Experimental setup

In order to explore the detonation acoustic characteristics of a PDE with an ellipsoidal reflector, the experiment system is set up as shown in Fig. 1. The experimental system consists of a PDE tube, fuel, and oxidizer supply apparatus, a control and ignition system, an acoustic measurement subsystem, and a data acquisition and processing subsystem. The PDE tube is constructed from a 304 stainless steel pipe with an inner diameter of 60 mm. The PDE tube is closed at one end and opened at the other end. By means of electromagnetic valves, liquid gasoline fuel is delivered into the head wall of the PDE tube then, along with compressed oxygen and compressed air as an oxidizer, it is injected into the mixing chamber from a tangential direction. For better mixing results of fuel and oxidizer, an atomizing spray nozzle is adopted to enhance the atomization and vaporization of the liquid fuel. Then a Venturi tube is employed to accelerate the flow for secondary atomization of liquid fuel droplets. Then the mixtures are ignited by a spark plug, which delivers an energy of 1.5 J to each spark. The operation frequency can be adjusted easily by a signal generator device. A Shchelkin spiral is inserted into the front of the detonation chamber to accelerate the deflagration-to-detonation transition (DDT) process. In the present work, the equivalence ratio of the fuel and oxidizer mixture is maintained at a stoichiometric value: $\phi = 1$. The fill fraction (ff) defined as the ratio of the volume of the detonation tube filled with a combustible mixture prior to ignition to the overall volume of the tube is kept at a constant of 1.0.

The acoustic measurement facility is specifically designed for obtaining acoustic data. A circular microphone array of six PCB model 377A12 microphones and 426B03 1/4" preamplifier are arranged at directivity angles of 0°, 20°, 40°, 60°, 75°, and 90° at a radius from 1 m to 50 m away from the PDE exit. The directivity angle is defined as the angle from the microphone with respect to the PDE tube centerline with 0° being assigned to be the downstream direction. The acoustic data of PDE are acquired at 500 k samples/s for all microphones simultaneously.

Figure 2 indicates the relevant definitions and geometry parameters for the ellipsoidal reflector used in this study. As shown in Fig. 2, half the length of the major axis a is 10.2 m and the minor axis b is 2 m, while c and h respectively represent half the focal length and the depth of the concave surface, whose values are 10 m and 1 m, respectively. The radius of the mouth plane r is 0.87 m. Focus point F_1 is the position of the PDE exit. After the shock wave is discharged from the PDE exit, it will arrive at the second focus point F_2 after serial reflections.

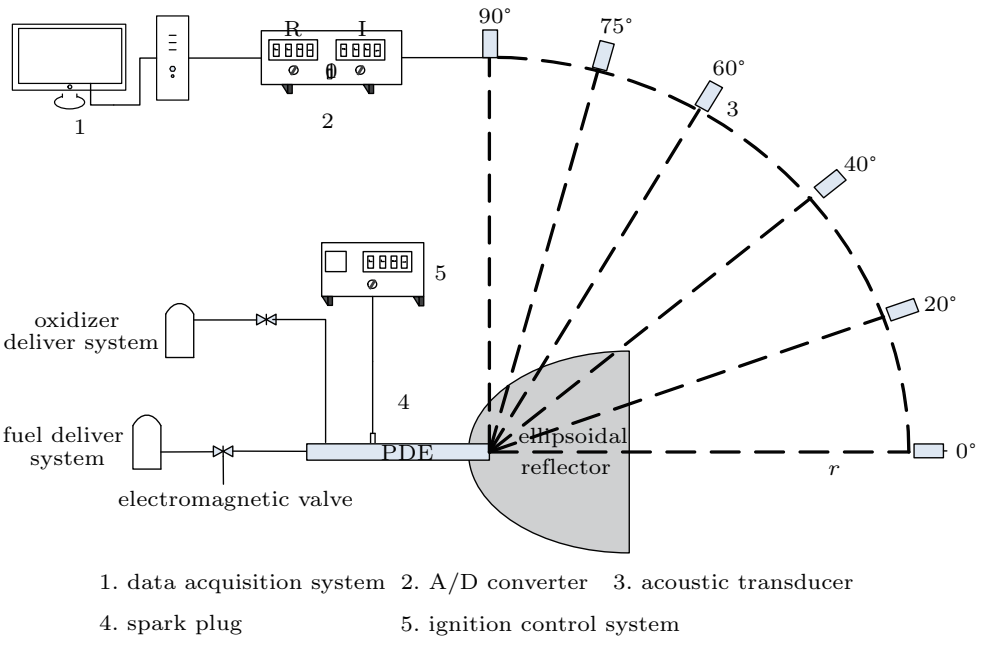


Fig. 1. Schematic diagram of experimental setup.

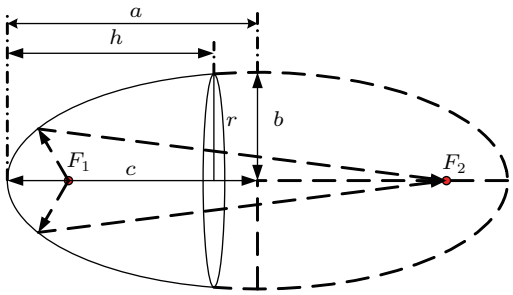


Fig. 2. Ellipsoidal reflector bunching mechanism.

It is noticed that there are two important acoustic parameters for various types of impulse noises, peak sound pressure level (PSPL), and overall sound pressure level (OASPL), the former (i.e. PSPL) is universally considered as the most critical factor for human noise-induced hearing loss and is defined as

$$\mathrm{PSPL} = 20\lg(P_{\mathrm{peak}}/P_0). \tag{1}$$

In formula (1), P_{peak} is the peak sound pressure of impulse noise and P_0 is the baseline sound pressure, which equals 2×10^{-5} Pa.

The latter (i.e. OASPL) is defined as

$$\mathrm{OASPL} = 20\lg(P_{\mathrm{RMS}}/P_0). \tag{2}$$

In formula (2), P_{RMS} is the effective sound pressure of impulse noise and is equal to

$$P_{\mathrm{RMS}} = \sqrt{\frac{1}{T}\int_0^{\mathrm{T}} p(t)^2\,\mathrm{d}t}. \tag{3}$$

The OASPL presents the amount of noise radiation energy, which is also an important factor for destroying human hearing.

2.2. Formulation of physical and numerical models

In order to explore the influence of flow field near the tube exit on PDE acoustic characteristics, a computational analysis model is established. The main difficulty in performing a simulation lies in the complex interaction between two phases of a two-phase detonation in the PDE tube. In this paper, a two-fluid model is chosen for the simulation of two-phase detonation.

To simplify the process of the gas/liquid two-phase detonation, it is assumed that the gas/liquid two-phase pulse detonation engine is axisymmetric in structure; the phase of droplets is considered as a continuous medium; the radii of droplets are uniform and the droplets are homogenously distributed initially; the interactions between droplets can be ignored; each droplet does not break and remains spherical while the detonation propagates; the initial temperature of the gas and the droplets are the same; the shape of each of the droplets always keeps spherical even in the process of separation and evaporation; and when the droplets reach the gaseous state, chemical reactions occur and are accomplished immediately.

Under the above assumptions, the Euler equations for compressible flows in gas/liquid two-phase PDE can be expressed in the conservative form as[17]

$$\frac{\partial \boldsymbol{U}}{\partial t} + \frac{\partial \boldsymbol{F}}{\partial x} + \frac{\partial \boldsymbol{G}}{\partial y} = \boldsymbol{R} - \frac{\boldsymbol{H}}{y}. \tag{4}$$

$$\boldsymbol{U}=\begin{bmatrix}\phi_{\rm g}\rho_{\rm g}\\ \phi_{\rm l}\rho_{\rm l}\\ \phi_{\rm g}\rho_{\rm g}u_{\rm g}\\ \phi_{\rm g}\rho_{\rm g}v_{\rm g}\\ \phi_{\rm l}\rho_{\rm l}u_{\rm l}\\ \phi_{\rm l}\rho_{\rm l}v_{\rm l}\\ \phi_{\rm g}\rho_{\rm g}E_{\rm g}\\ \phi_{\rm l}\rho_{\rm l}E_{\rm l}\end{bmatrix},\quad \boldsymbol{F}=\begin{bmatrix}\phi_{\rm g}\rho_{\rm g}u_{\rm g}\\ \phi_{\rm l}\rho_{\rm l}u_{\rm l}\\ \phi_{\rm g}(\rho_{\rm g}u_{\rm g}^2+p)\\ \phi_{\rm g}\rho_{\rm g}u_{\rm g}v_{\rm g}\\ \phi_{\rm l}(\rho_{\rm l}u_{\rm l}^2+p)\\ \phi_{\rm l}\rho_{\rm l}u_{\rm l}v_{\rm l}\\ \phi_{\rm g}u_{\rm g}(\rho_{\rm g}E_{\rm g}+p)\\ \phi_{\rm l}u_{\rm l}(\rho_{\rm l}E_{\rm l}+p)\end{bmatrix},$$

$$\boldsymbol{G}=\begin{bmatrix}\phi_{\rm g}\rho_{\rm g}v_{\rm g}\\ \phi_{\rm l}\rho_{\rm l}v_{\rm l}\\ \phi_{\rm g}\rho_{\rm g}u_{\rm g}v_{\rm g}\\ \phi_{\rm g}(\rho_{\rm g}v_{\rm g}^2+p)\\ \phi_{\rm l}\rho_{\rm l}u_{\rm l}v_{\rm l}\\ \phi_{\rm l}(\rho_{\rm l}v_{\rm l}^2+p)\\ \phi_{\rm g}v_{\rm g}(\rho_{\rm g}E_{\rm g}+p)\\ \phi_{\rm l}v_{\rm l}(\rho_{\rm l}E_{\rm l}+p)\end{bmatrix},$$

$$\boldsymbol{R}=\begin{bmatrix}I_{\rm d}\\ -I_{\rm d}\\ I_{\rm d}u_{\rm l}-F_{\rm dx}\\ I_{\rm d}v_{\rm l}-F_{\rm dy}\\ -I_{\rm d}u_{\rm l}+F_{\rm dx}\\ -I_{\rm d}v_{\rm l}+F_{\rm dy}\\ -Q_{\rm d}+Q_c-\left(F_{\rm dx}u_{\rm l}+F_{\rm dy}v_{\rm l}\right)+I_{\rm d}\left(E_{\rm l}+p/\rho_{\rm l}\right)\\ Q_{\rm d}+\left(F_{\rm dx}u_{\rm l}+F_{\rm dy}v_{\rm l}\right)-I_{\rm d}\left(E_{\rm l}+p/\rho_{\rm l}\right)\end{bmatrix},$$

$$\boldsymbol{H}=\begin{bmatrix}\phi_{\rm g}\rho_{\rm g}v_{\rm g}\\ \phi_{\rm l}\rho_{\rm l}v_{\rm l}\\ \phi_{\rm g}\rho_{\rm g}u_{\rm g}v_{\rm g}\\ \phi_{\rm g}\rho_{\rm g}v_{\rm g}^2\\ \phi_{\rm l}\rho_{\rm l}u_{\rm l}v_{\rm l}\\ \phi_{\rm l}\rho_{\rm l}v_{\rm l}^2\\ \phi_{\rm g}v_{\rm g}(\rho_{\rm g}E_{\rm g}+p)\\ \phi_{\rm l}v_{\rm l}(\rho_{\rm l}E_{\rm l}+p)\end{bmatrix}.$$

There is a constraint of the volume fraction for the two-fluid model: $\phi_{\rm g}+\phi_{\rm l}=1.0$, where g and l mean gas phase and liquid phase respectively, $\phi_{\rm g}$ and $\phi_{\rm l}$ denote the volume fraction ratio of the gas phase and liquid phase. In Eq. (4), p is the pressure, ρ the density, x the longitudinal distance, y the radial distance in a cylindrical coordinate, and u and v are the velocity components in the direction of the x and y axis respectively. The total energy density E of gas can be expressed as

$$E=e+\frac{1}{2}(u^2+v^2), \tag{5}$$

The value of $I_{\rm d}$ can be obtained to be[17]

$$I_{\rm d}=-n\rho_{\rm l}4\pi R^2\frac{{\rm d}R}{{\rm d}t}, \tag{6}$$

where

$$\frac{{\rm d}R}{{\rm d}t}=-\frac{1}{2}\sqrt{3\pi}\left(\frac{\rho_{\rm g}\mu_{\rm g}}{\rho_{\rm l}\mu_{\rm l}}\right)^{1/6}\left(\frac{\mu_{\rm l}}{\rho_{\rm l}}\right)^{1/2}\left|\boldsymbol{V}_{\rm g}-\boldsymbol{V}_{\rm l}\right|^{1/2}R^{-1/2}-\frac{3\lambda Nu\left(T_{\rm g}-T_{\rm l}\right)}{\pi R\rho_{\rm l}L}. \tag{7}$$

The first term on the right-hand side of Eq. (7) describes the evaporation of fuel drops, and the second term of $I_{\rm d}$ denotes the shattering of fuel drops. The force components on droplets are expressed as[17]

$$F_{{\rm d}x}=\frac{1}{2}n\pi R^2C_{\rm D}\rho_{\rm g}\left|\boldsymbol{V}_{\rm g}-\boldsymbol{V}_{\rm l}\right|\left(u_{\rm g}-u_{\rm l}\right), \tag{8}$$

$$F_{{\rm d}y}=\frac{1}{2}n\pi R^2C_{\rm D}\rho_{\rm g}\left|\boldsymbol{V}_{\rm g}-\boldsymbol{V}_{\rm l}\right|\left(v_{\rm g}-v_{\rm l}\right), \tag{9}$$

with

$$C_{\rm D}=\begin{cases}27Re^{-0.84}, & Re<80,\\ 0.27Re^{0.21}, & 80\le Re<10^4,\\ 2, & Re\ge 10^4,\end{cases} \tag{10}$$

$$Re=\frac{2\rho_{\rm g}\left|\boldsymbol{V}_{\rm g}-\boldsymbol{V}_{\rm l}\right|R}{\mu_{\rm g}}, \tag{11}$$

$$\left|\boldsymbol{V}_{\rm g}-\boldsymbol{V}_{\rm l}\right|=\left[\left(u_{\rm g}-u_{\rm l}\right)^2+\left(v_{\rm g}-v_{\rm l}\right)^2\right]^{1/2}, \tag{12}$$

where R is the radius of fuel droplets, λ the heat conduction coefficient of gas, L the heat of the evaporation of fuel droplets, $\mu_{\rm g}$ and $\mu_{\rm l}$ the viscosity coefficient of the gas phase and droplet phase, respectively, $C_{\rm D}$ is the drag coefficient, Nu the Nusselt number, Re the Reynolds number, Pr the Prandtl number, and $Q_{\rm d}$ and $Q_{\rm f}$ are the convection heat conduction between two phases and the chemical reaction heat, respectively.

Equation (4) is solved numerically using a two-dimensional (2D) non-splitting unstructured triangular mesh Euler solver on the CE/SE method developed by Wang and Chang.[18,19] For the problem of the chemical reaction source term, the source is rigid due to the characteristic time of the chemical reaction being far less than the characteristic convection time. A fourth order Runge–Kutta (RK) method is used to deal with the source term. Firstly, the CE/SE method is used to solve $(\boldsymbol{U})_j^n$ without considering the effect of the source term. Secondly, as an initial value, $(\boldsymbol{U})_j^n$ is used to solve the ordinary differential equations ${\rm d}\boldsymbol{U}/{\rm d}t=\boldsymbol{R}$. Time step in the fourth order Runge–Kutta method is shown as follows:

$$\Delta t_{\rm R-K}=\frac{\Delta t_{\rm CE}}{2N}. \tag{13}$$

Figure 3 shows the computational domain and boundary conditions used in the computation. The PDE walls and ellipsoidal reflector are considered as solid wall conditions. Since the flow field is symmetric, the region above the symmetric line is used as the computational domain. The symmetric conditions are imposed on the centerline of the PDE. The outlet of the PDE uses the non-reflective freedom boundary condition of the CE/SE method. The boundaries of the external flow field use the outflow boundary conditions. The entire computational domain is divided by unstructured triangular meshes.

The initial pressure and temperature are 1 atm (the unit 1 atm = 1.01325×10^5 Pa) and 298 K respectively. Gasoline/air mixture at a certain stoichiometric ratio is filled uniformly in the PDE tube. The radius of fuel droplets is 50 μm.[20] In order to simulate the initial ignition spark, 15 ambient pressures and 15 ambient temperatures are specified in the range of $x/l\le0.01$ and $r/r_0\le0.5$,[21,22] where l is the length of the tube and r_0 is the radius of the tube. The external flow field is filled with air at the normal temperature and pressure.

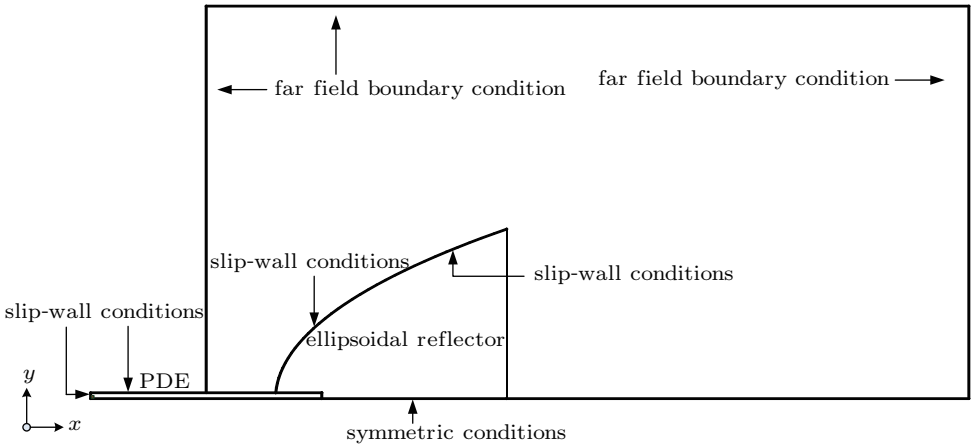


Fig. 3. Computational domain and boundary conditions.

3. Formation process and characteristic analysis of PDE sound

The PDE sound is essentially produced through two sources: noise associated with shock wave and jet noise produced during the blowdown of the detonation products. Figure 4 shows four snapshots of the pressure contour after the detonation wave has left the PDE exit. When the detonation wave leaves the detonation tube exit, it rapidly degenerates to a bow shock. With the shock wave propagating, the shock wave attenuates into shock noise. Then the high-pressure detonation products in the wake of the detonation wave quickly expand in a spherical manner forward in the PDE tube. The leading edge of the detonation produces a jet that interacts with the ambient atmosphere to form a shock front. The jet noise consists of the jet shock noise and jet turbulence noise.

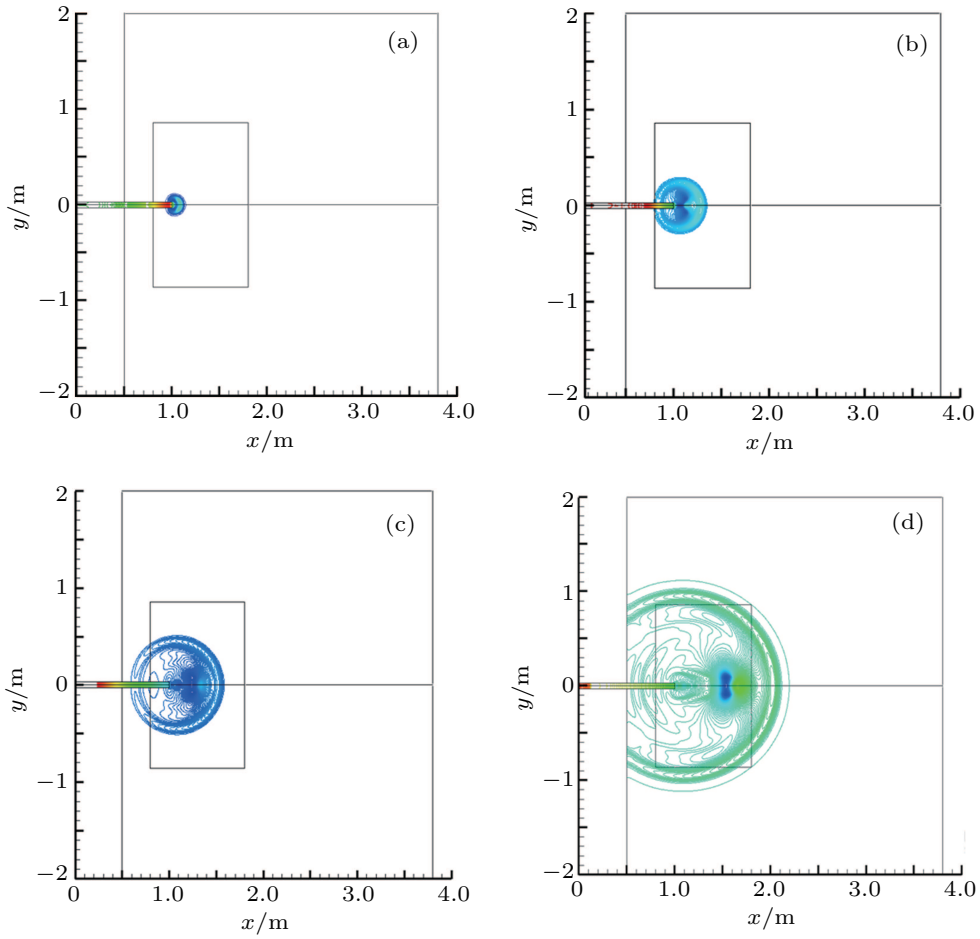


Fig. 4. (color online) Four snapshots of the pressure contour of PDE external flow field at $t = 1.18$ ms (a), 1.2 ms (b), 1.8 ms (c), and 3.3 ms (d).

Figure 5(a) shows the experimental results of sound pressure of the PDE in the 0°direction at the position 20 m away from the PDE exit under the condition of 5 Hz operation frequency. Figure 5(b) shows one pulsed sound pressure of PDE sound. As shown in Fig. 5(b), the first positive peak P_1 is 607.3 Pa, which represents the shock noise. When the weak shock wave passes through the testing position, the sound pressure rise quickly. A lower positive pressure peak comes after 0.28 ms and the second positive pressure peak P_2, which represents the jet noise, is about 221.8 Pa. A compensating negative phase is fully developed as shown in Fig. 5(b). The figure also shows that the ground reflection noise P_3 is 279.2 Pa delayed by 0.586 ms relative to shock noise.

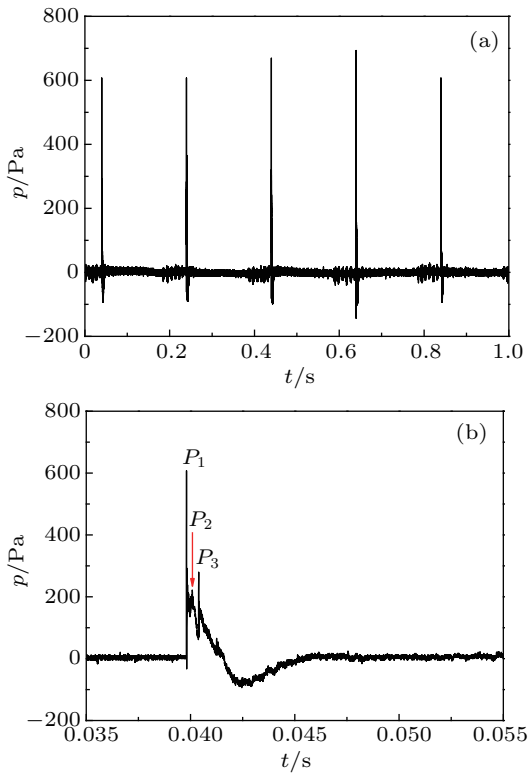


Fig. 5. (color online) Experimental results of sound pressure of PDE, showing (a) sound pressure of PDE sound and (b) impulse noise pressure history.

The sound pressure signal is analyzed by the FFT method. Figure 6 shows the logarithmic Fourier spectrum of pulse detonation acoustic characteristics. It can easily be found that the acoustic frequency spectrum is broad and the frequency ranges from 0 Hz to 10^5 Hz. However, the energy of acoustic radiation mainly concentrates in the frequency ranging from 0 Hz to 5×10^4 Hz. Figure 7 shows the cumulative fractional power for the pulse detonation acoustic power. The 90% of cumulative fractional power can be seen at 42857 Hz from Fig. 7. The analysis of the noise frequency spectrum shows the low frequency characteristic of PDE sound obviously and the characteristic keeps similar when the PDE works at the operation frequency of 10 Hz.

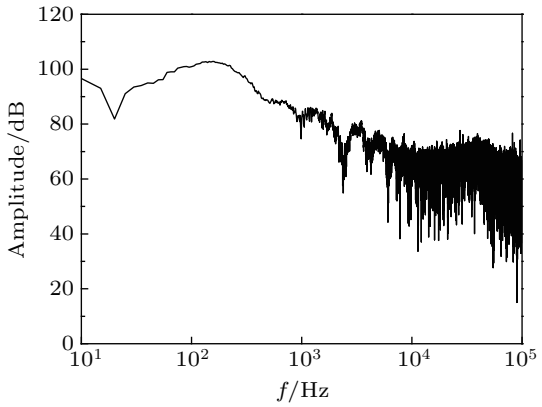


Fig. 6. Logarithmic acoustic spectrum.

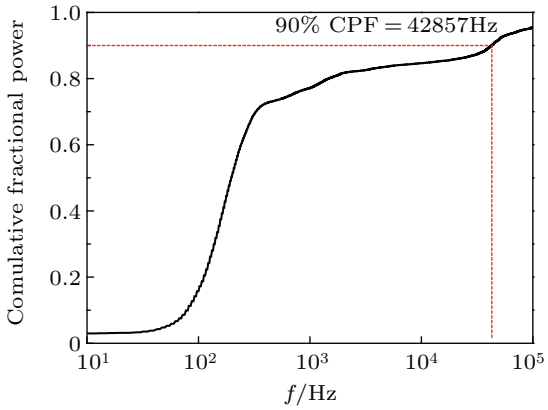


Fig. 7. (color online) Integrated fractional acoustic power as a function of frequency.

4. Effect of ellipsoidal reflector on flow field characteristics near PDE exit

The flow field structure near the PDE exit has a great influence on the formation of a PDE sound wave, so it is necessary to explore the flow field in the near-field region of the PDE. Figure 8 shows the predictions of the pressure contour of the PDE ellipsoidal reflector at 0.63 ms, 1.18 ms, 2.41 ms, 4.47 ms, and 5.80 ms. At 0.63 ms, the detonation wave is formed inside the PDE tube. Then the detonation wave discharge from the PDE tube exit forms a spherical wave at the external flow field. At 1.18 ms, the shock wave propagates to the reflector surface. With the increase of time, part of the shock wave and jet shock wave propagate further downstream as a direct wave without contacting the reflector. However, the wave propagating upstream is reflected by the ellipsoidal reflector resulting in the change of propagation direction. At 2.41 ms, the direct wave already propagates to the exit of the reflector while the reflected wave lags behind 0.5 m in the reflector region. As shown in Fig. 8(d), when it comes to 4.47 ms, the reflected wave propagates to the exit of the reflector and the wave is reflected. The edge waves are generated by the diffraction of the shock wave in the sharp corners of the

reflection surface, and the spherical diffraction waves centered in the sharp corners advance toward the PDE axis. In Fig. 8(e), the direct shock wave and jet shock wave are denoted as 1 and 2 while the reflected shock wave and reflected jet shock wave are marked as 3 and 4. Figure 8 shows the external flow field structure of the PDE with an ellipsoidal reflector in detail, which clearly demonstrate the formation process of the reflected shock wave and jet shock wave.

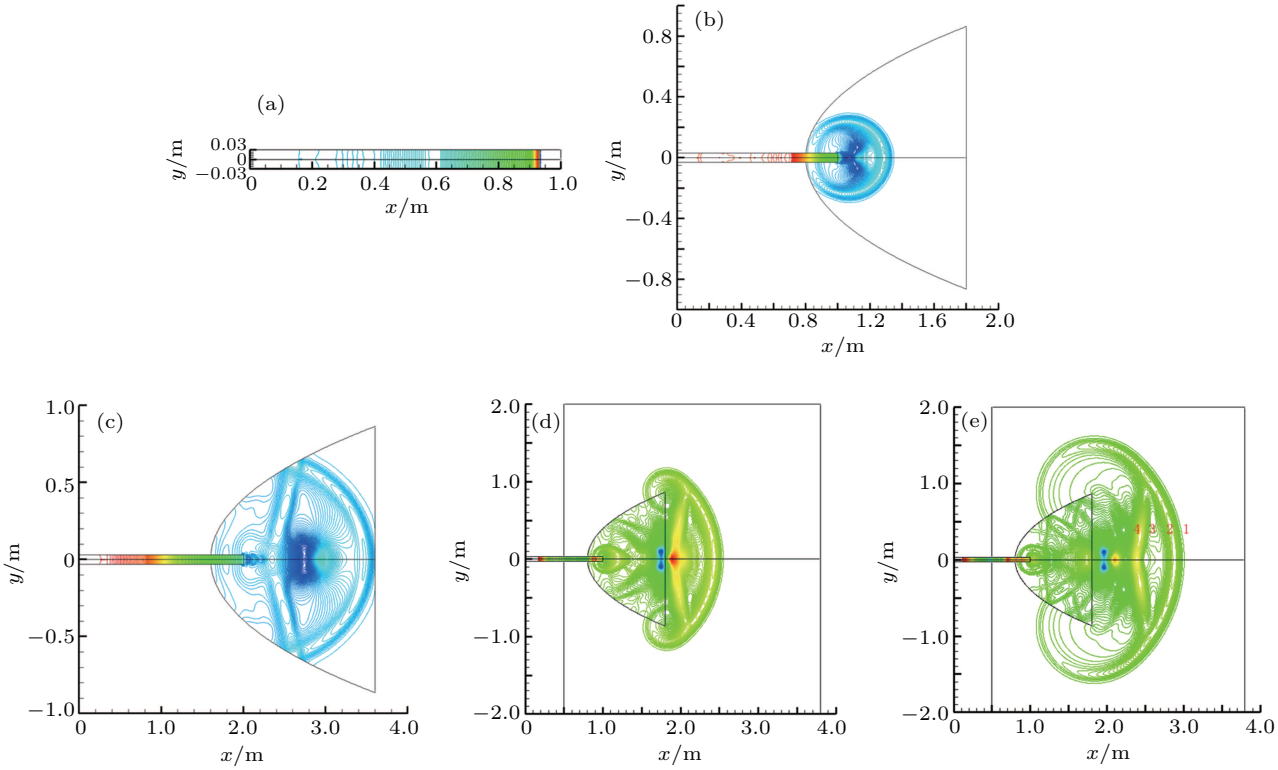


Fig. 8. (color online) Pressure contour PDE with reflector at $t = 0.63$ ms (a), 1.18 ms (b), 2.41 ms (c), 4.47 ms (d), and 5.80 ms (e).

5. Effect of ellipsoidal reflector on PDE sound

5.1. Effect of ellipsoidal reflector on PDE sound waveform

The first study conducted is to directly compare the acoustic time domain characteristics of PDE and PDE with an ellipsoidal reflector. In the experiments, the equivalence ratio of the fuel and oxidizer mixture, fill fraction, and the operation frequency keep consistent.

Figure 9(a) shows the comparison of time histories of the PDE acoustic noise at focus point F_2, which is in the 0° direction at the position 20 m away from the PDE exit when the PDE operates at 5 Hz. It is obvious to find that the installation of an ellipsoidal reflector can greatly enhance the sound pressure of the PDE. The sound pressure spikes are all around 1500 Pa when the PDE installs the reflector in contrast to 500 Pa of the PDE. The reflection and focus function of the ellipsoidal reflector can account for the sound pressure increment. Figure 9(b) shows the detailed view of the acoustic waveform of the PDE with a reflector. It differs from the PDE's which is shown in Fig. 5(b). As shown in Fig. 9(b), five obvious peaks exist, marked as P_1, P_2, P_3, P_4, and P_5. After the detonation wave discharges from the PDE exit at focus point F_1, it degrades to a near-spherical shock wave propagating radially outward. The shock wave and strong jets traveling in the direction of the PDE downstream axis propagate to the focus point F_2 directly. According to the surface characteristics of the ellipsoidal reflector, when the shock wave is traveling to the PDE upstream and propagates to the reflector, most of the energy is reflected.

Like the acoustic characteristics of the PDE, sound pressure peaks P_1 and P_2 represent the direct wave of shock noise and jet noise, respectively. P_3 is the ground reflection noise. Sound pressures P_4 and P_5 represent the wave produced by the reflecting and focusing of shock noise and jet noise. The direct shock noise propagates to the focus point F_2 ahead of the reflecting shock noise by 0.86 ms and the direct jet noise arrives at F_2 ahead by 2.13 ms compared with the reflecting jet noise. The reason for this phenomenon is the differences in the propagation distance and time of direct wave and reflection wave. However, the value of the focusing shock noise P_4, which is 1265.8 Pa, is about 3.7 times that of the direct shock noise. Numerical simulation results show that the focusing shock noise is 3.26 times direct shock noise at 2 m away from the PDE exit. The experimental results show that the focusing shock noise at this testing point is 3.04 times the direct shock noise, which is consistent with the numerical simulation. Due to the limitation of the computational area, the focusing noise

and direct noise cannot be calculated at the position of 20 m away from the PDE exit directly, but the calculation results of the linear model of an acoustic wave show that the numerical calculation in the far field is also consistent with the simulation result. The value of focusing jet noise P_5 is 539.9 Pa, which is about 2.5 times that of the direct jet noise. As can be seen, there are minor oscillations following the peak pressure P_5. This may be caused by the complex flow field structure in the PDE plume.

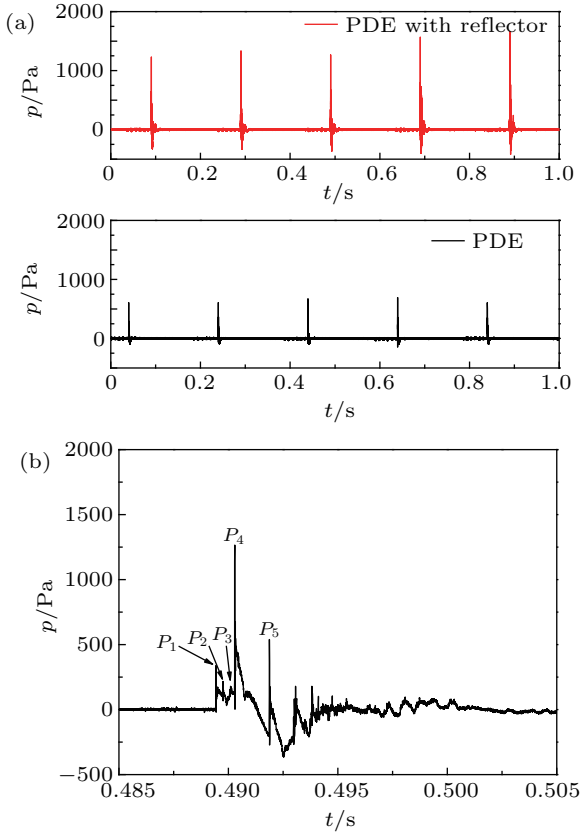


Fig. 9. (color online) (color online)Experimental results of sound pressure of PDE with ellipsoidal reflector, showing (a) comparison of time histories of PDE noise, and (b) sound pressure trace of the PDE with a reflector.

5.2. Effects of ellipsoidal reflector on PSPL and OASPL of PDE

Figure 10 plots the variations of PSPL and OASPL along the PDE axis. It is found that, no matter whether an ellipsoidal reflector is installed on the PDE, the PSPL and OASPL decrease rapidly with the rise of distance, but the attenuation rate gradually slows down. However, it can be noted that the installation of an ellipsoidal reflector contributes to the increase of PSPL and OASPL.

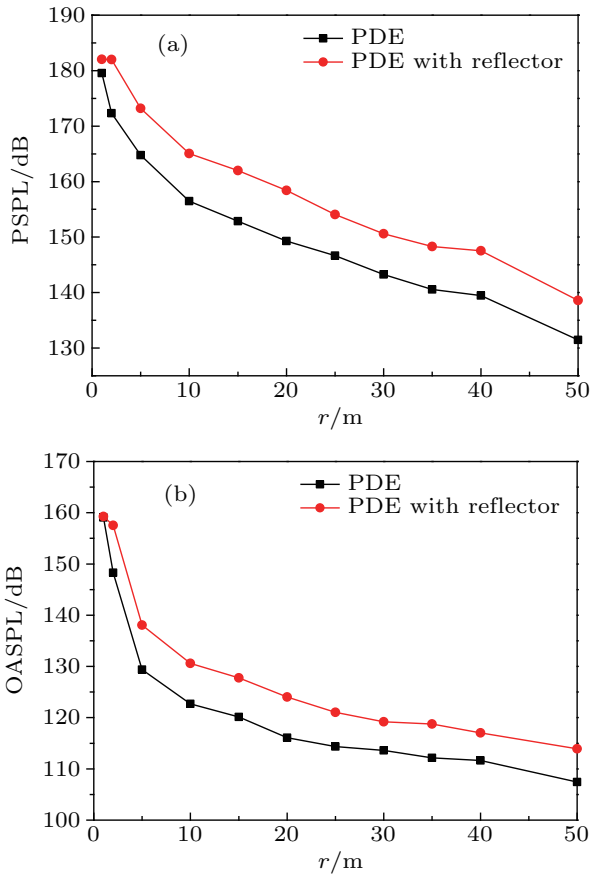


Fig. 10. (color online) (a) PSPL and (b) OASPL of PDE sound.

Table 1. Effect of ellipsoidal reflector on PSPL and OASPL.

Testing point	r/m	Increment of PSPL/dB	Relative increment ratio of PSPL/%	Increment of OASPL/dB	Relative increment ratio of OASPL/%
TP_1	1	2.49	1.39	0.18	0.11
TP_2	2	9.67	5.61	9.24	6.23
TP_3	5	8.42	5.11	8.70	6.72
TP_4	10	8.57	5.48	7.87	6.41
TP_5	15	9.13	5.97	7.64	6.36
TP_6	20	9.11	6.10	7.94	6.84
TP_7	25	7.44	5.07	6.70	5.86
TP_8	30	7.32	5.11	5.57	4.90
TP_9	35	7.73	5.50	6.60	5.88
TP_{10}	40	8.08	5.80	5.39	4.83
TP_{11}	50	7.14	5.43	6.46	6.01

The calculated results of the increase and relative increase ratio of PSPL and OASPL of the PDE by the reflector are presented in Table 1. It can be found that with the reflector installed, the PSPL and OASPL increase to different degrees. The values of the increase of PSPL and OASPL in the range from 1 m to 50 m are about 2.5 dB to 9.7 dB and 0.2 dB to 9.2 dB, respectively. The values of the relative increase ratio of PSPL and OASPL are 1.4% to 6.1% and 0.1% to 6.8%. In the process of PDE sound attenuation from near field to far field, the variation of the sound pressure level is not linear. As a result, the increase of PSPL and OASPL cannot reflect the actual effect of the ellipsoidal reflector on the noise focusing. The maximum increase of PSPL and OASPL are obtained at TP_2, whose values are 9.67 dB and 9.24 dB, while the maximum relative increase ratio of PSPL and OASPL are obtained at TP_6, whose values are 6.1% and 6.84% respectively. Testing point P_6 is at the position of focus point F_2, which means that the focus point F_2 is the focusing point on the centerline of the ellipsoidal reflector, which is exactly as designed.

5.3. Effect of ellipsoidal reflector on directivity of PDE sound

From the above analysis, it can be seen that the radiation energy of PDE sound has significant differences in different directions. The research on the directivity of PDE sound is of great significance for designing the structure of PDE. A thorough understanding of PDE sound directivity is beneficial to controlling the emission angle of sound for better utilization.

To simplify the study of the variation of directivity of PDE sound, the PSPL of PDE noise is normalized as

$$\overline{P_r^\theta} = \frac{P_r^\theta}{P_r^{0^\circ}},$$

where r is the distance from the PDE exit, θ is the angle, P_r^θ is the PSPL of PDE noise at r away from the PDE exit at the directivity angle θ, and $\overline{P_r^\theta}$ is the dimensionless quantity of P_r^θ after normalization.

The corresponding PSPL at different angles of PDE sound are shown in Figs. 11(a) and 11(b). As observed in Fig. 11(a), the greatest PSPL of PDE sound appears at a directivity angle of 20°. PSPL at 0° is close to 90° at focus point F_2. The PDE sound exhibits quadrupole characteristics. However, Fig. 11(b) shows that the greatest PSPL changes to the 0° directivity angle, with the reflector installed. The PSPL at a 0° angle is at least 5 times the PSPL at a 90° angle and twice the PSPL at 20°. The ellipsoidal reflector reflects and focuses the sound energy near the axis of the reflector. This suggests that the reflector has a significant change in the acoustic characteristic of PDE sound.

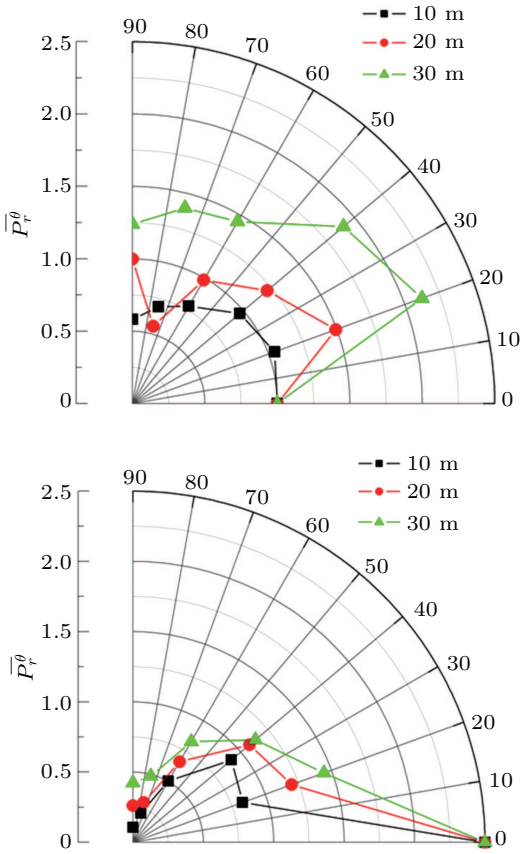


Fig. 11. (color online) Directivity of PDE sound, showing (a) directivity angle on PSPL of PDE, and (b) directivity angle on PSPL of PDE with reflector.

5.4. Effect of ellipsoidal reflector on duration of PDE sound

Hearing impairment and loudness are both related to the energy of impulse noise. When evaluating the energy of impulse noise, the effective duration and the amplitude of sound pressure are equally important. Therefore, the duration becomes another important physical characteristic. Three types of durations are commonly used to assess impulse noise, i.e., A duration (t^+), B duration (t_B), and C duration (t_C). The A duration is the time taken for the initial or principal pressure wave to rise to its positive peak and return momentarily to ambient pressure. The B duration is the total time taken for the envelope of the pressure fluctuations (positive and negative) to be within 20 dB of the peak pressure level.[23] Referring to the definition of impulse noise duration, the A duration and B duration of PDE sound are studied in this research.

Figure 12 shows the A duration and B duration of PDE sound at the focus point F_2. It can be seen that t_1^+ and t_{B1} of PDE sound are 1.764 ms and 3.613 ms, respectively. The t_2^+ and t_{B2} of the sound of PDE with reflector are 1.923 ms and 4.337 ms, respectively. It suggests that the installation of an ellipsoidal reflector contributes to an increment of 0.159 ms of A duration and 0.724 ms of B duration. By analyzing the waveform in Fig. 12, the t^+ and t_B of the PDE sound are determined by the shock noise and jet noise. Due to the focusing

wave generated by the ellipsoidal reflector, the time of acoustic pressure beginning to fall is delayed and this results in the increment of A duration and B duration.

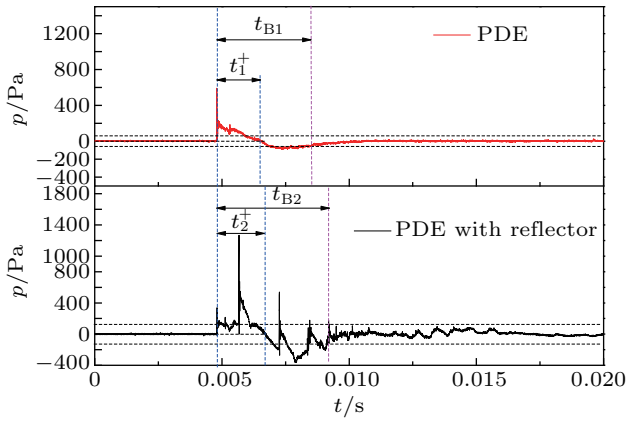


Fig. 12. (color online) t^+ and t_B of sound of PDE and PDE with reflector.

The A duration and B duration of PDE sound at different axial positions are shown in Figs. 13(a) and 13(b). It can be noted that the variation rule of A duration and B duration of the sound of PDE with the reflector are similar to the rule of PDE sound.

As shown in Fig. 13(a), t_2^+ is larger than t_1^+ except from 1 m to 2 m. In the near-field region, the propagation velocity of the shock wave formed by the detonation wave is very fast, the time taken for the reflection wave to arrive at the test point is quite different from the time taken for the direct wave to reach the test point. When the reflection wave arrives at the test point, the direct wave pressure decreases to a negative value. The A duration of PDE sound in the near-field is only determined by the direct wave. As a result, it can be seen that t_1^+ is close to t_2^+ from 1 m to 2 m. In the far-field region, the shock wave degrades into a sound wave and the propagation velocity of direct wave decreases. The A duration of PDE sound in the far-field is determined by the direct wave and reflection wave. As a result, t_2^+ is larger than t_1^+ in the far-field region of the PDE.

It can also be noted that t_1^+ and t_2^+ achieve a sharp increase at an axial position 1 m to 10 m away from the PDE exit. However, in the range from 10 m to 50 m, the increasing rate slows down. According to the analysis, the acoustic energy of a certain amount of impulse sound passing through the unit area decreases as the axial distance increases, thus the peak sound pressure decreases, the pressure-time curve widens, and the A duration also increases.

As shown in Fig. 13(b), t_{B1} and t_{B2} both decrease rapidly from 2 m to 5 m. In the range from 5 m to 50 m, t_{B1} fluctuates in the range of 3.4 ms to 5.3 ms, and t_{B2} fluctuates in the range of 4.3 ms to 5.3 ms. It can be found that t_{B1} is getting close to t_{B2} at the axial position after 30 m. This suggests that the ellipsoidal reflector can increase the B duration of PDE sound before and near the focus point F_2, but it has no effect on the position away from the focus point F_2. This can also suggest that the influence of installing an ellipsoidal reflector on the hazardous range of PDE sound is limited.

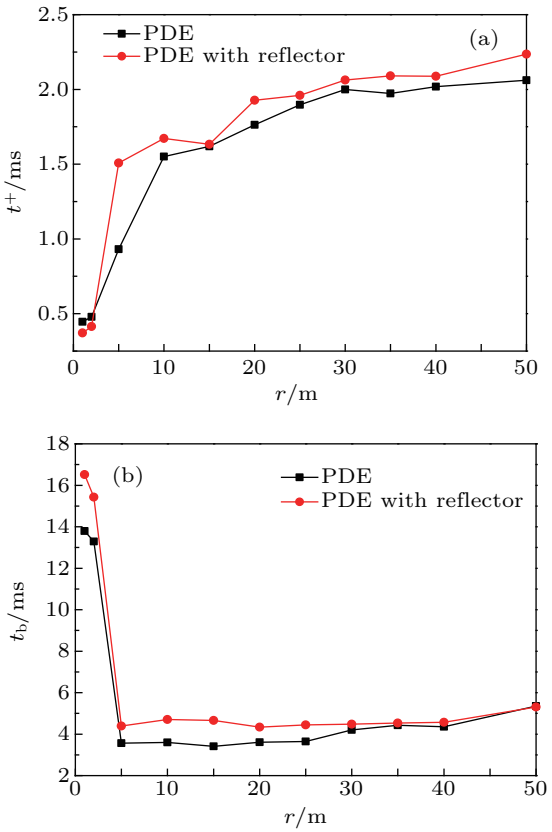


Fig. 13. (color online) A duration and B duration of PDE sound at different axial positions, showing (a) t^+ and (b) t_B of the noise of PDE sound in different r values.

6. Conclusions

In this study, the acoustic characteristics of a PDE with and without an ellipsoidal reflector are numerically and experimentally investigated. The formation process of PDE sound is explored by the computational analysis. The PDE sound is essentially produced through two sources: noise associated with a shock wave and jet noise produced during the blowdown of the detonation products. The numerical results clearly demonstrate the flow field structure near the exit of the PDE with an ellipsoidal reflector. The shock wave and jet shock wave originally propagating upstream are reflected by the ellipsoidal reflector and focused in the PDE axis direction. The experimental results show that the ellipsoidal reflector can realize the shock wave noise and jet noise focusing well, and create a focal zone at the PDE axis with very high pressure, and obviously slow down the pressure attenuation along the distance and time in the downstream direction. The maximum relative increase ratio of PSPL and OASPL are obtained at focus point F_2 of the ellipsoidal reflector, whose values are 6.1% and 6.84% respectively. The greatest PSPL of PDE sound appears at a directivity angle of 20° while it changes to 0° direc-

tivity angle under the installation of the reflector. Due to the focusing wave generated by the ellipsoidal reflector, the time of acoustic pressure beginning to fall turns delayed, resulting in the increase of A duration and B duration before and near focus point F_2.

References

[1] Kailasanath K 2003 *AIAA J.* **41** 145

[2] Boesch H E, Christian G R and Bruce T B 2000 *Army research lab adelphi* MD No. ARL-TR-2203

[3] Allgood D, Glaser A, Caldwell N and Gutmark E 2004 10*th AIAA/CEAS AeroAcoust. Conference*, May 2004 (Manchester, Great Britain), p. 2879

[4] He X and Karagozian A R 2004 42*nd AIAA Aerosp. Sci. Meeting Exhibit*, January 5–8, 2004, Reno, USA, p. 469

[5] Shaw L, Harris K, Schauer F and Hoke J 2005 11*th AIAA/CEAS AeroAcoust. Conference*, May 23–25, 2005, Monterey, USA, p. 2952

[6] Glaser A, Caldwell N and Gutmark E 2006 12*th AIAA/CEAS AeroAcoust. Conference* May 8–10, 2006, Cambridge, USA, p. 2453

[7] Caldwell N, Glaser A and Gutmark E 2006 44*th AIAA Aerosp. Sci.Meeting Exhibit*, January 9–12, 2006, Reno, USA, p. 1233

[8] Zheng L X, Li N and Yan C J 2009 47*th AIAA Aerosp. Sci. Meeting Including The New Horizons Forum Aerosp. Exposition*, Janurary 5–8, 2009, Orlando, USA, p. 297

[9] Xu G Y, Weng C S, Li N and Huang X L 2016 *Int. J. Turbo. Jet Eng.* **33** 19

[10] Glaser A, Caldwell N and Gutmark E 2007 45*th AIAA Aerosp. Sci. Meeting Exhibit*, January 8–11, 2007, Reno, USA, p. 444

[11] Ben-Dor G, Igra O and Elperin T 2001 *Handbook Shock Waves*, Vol. 2 (London: Academic Press) pp. 397–414

[12] Wilbert D M 2002 *Bju Int.* **90** 507

[13] Cates J E and Sturtevant B 1997 *Phys. Fluids* **9** 3058

[14] Sturtevant B and Kulkarny V A 1976 *J. Fluid Mech.* **73** 651

[15] Schaefer R and Grapperhaus M 2006 *Defense Security Symposium*, May 12, 2006, Orlando, USA, p. 621901

[16] Zhou Y F and Zhong P 2006 *J. Acoust. Soc. Am.* **119** 3625

[17] Wang G, Zhang D L, Liu K X and Wang J T 2010 *Comput. Fluids* **39** 168

[18] Chang S C 1995 *J. Comput. Phys.* **119** 295

[19] Wang X Y and Chang S C 1999 *Comput. Fluid Dyn. J.* **8** 309

[20] Ma D H and Weng C S 2010 *J. Chin. Ordnance* **6** 05

[21] Weng C S and Gore J P 2005 *Acta Mech. Sin.* **21** 32

[22] Shen Y, Shen H, Liu K X, Chen P and Zhang D L 2016 *Chin. Phys. B* **25** 114702

[23] Coles R R A, Garinther G R and Hodge D C 1968 *J. Acoust. Soc. Am.* **43** 336